CHAPTER VI
STEAM REFORMING OF TOLUENE AS A MODEL COMPOUND OF TAR DERIVED FROM BIOMASS GASIFICATION: THE EFFECT OF TRANSITION METAL OXIDE DOPING

6.1 Abstract

In this study, the catalytic activity of nickel supported on $Ce_{0.75}Zr_{0.25}O_2$ and $Ce_{0.75}Zr_{0.15}Me_{0.10}O_2$ (Me = Cr, Fe, Mn and V) mixed oxide catalysts prepared by urea hydrolysis and incipient wetness impregnation was investigated for steam reforming of toluene selected as a model compound of biomass-derived tar. The results showed that the nickel supported on transition metal oxide-doped CeO_2-ZrO_2 catalyst exhibit good activity and stability for toluene steam reforming. Moreover, the incorporation of transition metal oxide, in particular Mn, into CeO_2-ZrO_2 which is used as support was found to improve the performance of the Ni-based catalyst for carbon formation resistance due to its high reducibility and oxygen mobility, resulting in promoting the gasification of deposited carbon.

6.2 Introduction

Thermochemical conversion technologies, pyrolysis, gasification and combustion, are especially useful to produce fuels, chemicals, combined heat and power with high-energy efficiencies. Among them, biomass gasification has attracted a lot of interest by producing a gas rich in CO and H_2 used for methanol or Fischer-Tropsch synthesis, chemical production or electricity generation (turbine, gas engine or fuel cells). Despite extensive research efforts, tar formation is still a major problem in biomass gasification systems. The condensable compounds present in tar may cause problems in downstream equipment, making catalytic hot gas conditioning a necessary step in most gasification application (Dayton *et* al. 2002; Abu El-Rub *et al.* 2004). The catalytic steam reforming is one attractive technique for tar removal.

Several kinds of catalysts were developed and applied in this process. A recent review by Sutton *et al.* (Sutton *et al.* 2001) summarizes the current status of catalysts in gasification gas cleaning. Until now, the research in this field has mainly focused on nickel-based steam-reforming catalysts. Nickel catalysts are active in decomposition of tar and have been studied by many research groups (Baker *et al.* 1987; Chen *et* al, 2008; Furusawa *et al.* 2009; Li *et al.* 2009). Nickel catalysts also decompose light hydrocarbons, which with their high heating value are useful components in many combustion applications. Unfortunately, nickel catalysts are easily deactivation due to carbon deposited has been reported (Baker *et al.*, 1987; Garcia *et al.*, 2000). Carbon formation is regarded as one main problem for deactivation of Ni-based catalysts, because during biomass gasification process, complex hydrocarbons steam reforming reactions are included, which involves a risk of carbon deposition.

Several attempts have been made to promote the long-term stability of steam-reforming catalysts. One of the most effective ways to reduce and/or prevent the carbon poisoning is the development of the catalyst support. Several catalyst supports such as dolomite, olivine, MgO and MgO-CaO were reported (Sato *et al.*, 2007; Świerczyński *et al.*, 2007; Miyazawa *et al.*, 2006; Srinakruang *et al.*, 2006). It was recently found that the catalysts based on CeO_2-ZrO_2 possess good performance in reforming of hydrocarbons due to high oxygen storage capacity and a high oxygen mobility in its lattice which provide a advantage for carbon formation resistance (Pengpanich *et al.*, 2004; Chen *et al.*, 2008; Park *et al.*, 2009).

Generally, one of the important routes to further improve the catalytic performances of ceria-based material is by doping and modification with other elements. The addition of dopants can increase the concentration of oxygen vacancies and/or improve the thermal stability of the parent oxide. The dopant caions with ionic radius and electronegativity close to those of cerium cation are thought to be the most appropriate modifiers of structural and chemical properties of ceria (Etsell *et al.*, 1970). The similarity of the ionic radii is also the criterion to predict the presence or not of significant solid solubility. In our previous study, we found that the incorporation of manganese ions into the ceria lattice would improve the oxygen storage capacity and the oxygen mobility on the surface of mixed oxides, resulting in

enhancing the carbon deposited gasification (Bampenrat *et al.*, 2009). This leads us to investigate the effect of doping the other transition metal oxides, such as chromium, iron, manganese, and vanadium, on the steam reforming catalytic activity of toluene as a tar compound model over nickel supported on $Ce_{0.75}Zr_{0.15}Me_{0.10}O_2$ (Me = Cr, Fe, Mn and V) mixed oxide catalysts.

6.3 Experimental

6.3.1 Catalyst preparation

The series of mixed oxide samples $Ce_{0.75}Zr_{0.25}O_2$ and $Ce_{0.75}Zr_{0.15}Me_{0.10}O_2$ (Me = Cr, Fe, Mn and V) were prepared via urea hydrolysis. $Ce(NO_3)_3{\cdot}6H_2O$, $ZrOCl_2{\cdot}8H_2O$, $Cr(NO_3)_3{\cdot}9H_2O$, $Fe(NO_3)_3{\cdot}9H_2O$, $Mn(NO_3)_2{\cdot}4H_2O$ and NH_4VO_3 were used as sources of Ce, Zr,Cr, Fe, Mn and V, respectively. The starting solution was prepared by mixing 0.1 M of metal salts solutions with 0.4 M of urea solution at a 2 to 1 volumetric ratio. The synthesis procedures of catalysts have been reported elsewhere (Pengpanich *et al.*, 2002). Supported Ni catalysts (Ni = 15 wt%) were prepared by the incipient wetness impregnation method using $Ni(NO_3)_2$ solution. The samples were dried and calcined at 500 °C for 4 h. A Ni/Al_2O_3 catalyst was also prepared for comparison purposes.

6.3.2 Catalyst characterizations

The crystalline structure of the catalysts was analyzed by means of X-ray powder diffractometer (Rigagu) equipped with a RINT 2000 wide-angle goniometer using Cu Kα radiation (λ = 0.15059 nm.). The X-ray was operated at 40 kV and 100 mA. The mean particle diameter of CeO_2 was calculated from the X-Ray line broadening of the (111) diffraction peak according to Scherrer's equation.

The specific surface area, the pore volume and the pore size distribution of the samples were determined from adsorption and desorption isotherms of nitrogen at -196 °C using a Micromeritics modeled ASAP 2020 instrument. Prior to the measurements, the samples were outgassed to eliminate volatile adsorbents on the surface at 350 °C under vacuum.

H_2-Temperature programmed reduction (H_2-TPR) measurements were carried out to investigate the redox properties over the resultant materials. H_2 was used as a reducing gas. H_2-TPR was carried out in a TPR analyzer (Quantachrome modeled ChemBET-3000 TPR/TPD) using 50 mg of sample. The sample was pretreated in flowing N_2 (20 ml min^{-1}) at 250 °C for 30 min prior to running the TPR experiment, and then cooled down to room temperature in N_2. Then, the sample was exposed to a 5% H_2 in N_2 gas mixture at a flow rate of 75 ml min^{-1}, and the sample temperature was raised at a constant rate of 10 °C min^{-1} from room temperature to 1,100 °C. The amount of H_2 consumption during the increasing temperature period was determined by using a TCD signal.

The degree of nickel dispersion was determined by H_2 pulse chemisorption (Quantachrome modeled ChemBET-3000 TPR/TPD) at 50 °C using an N_2 flow of 75 ml min^{-1} and pulse of 0.1 ml (10% H_2 in N_2). For these measurements, approximately 500 mg of sample was placed in a quartz reactor. Prior to pulse chemisorption, the sample was reduced at 500 °C using pure H_2 for 1 h. Then the sample was purged with N_2 at 500 °C for 30 min and cooled to 50 °C in flowing N_2. A H_2 pulse was injected, the pulse was given 6-8 min intervals until the area of successive hydrogen peak were identical. The metal dispersion was calculated by assuming the adsorption stoichiometry of one hydrogen atom per nickel surface atom.

The morphology of the catalysts was observed by transmission electron microscopy (TEM) with a JEOL (JEM-2010) transmission electron microscope operated at 200 kV. Specimens were prepared by ultrasonically suspending the sample in ethanol. A drop of the suspension was then applied onto clean holy copper grids and dried in air.

The amount of deposited carbon on the spent catalysts was carried out using a TG7 Perkin-Elmer thermogravimetric analyzer. The standard involved the weight change of the sample (10 mg) during its heating in 100 ml min^{-1} of N_2 as purge gas and 10 ml min^{-1} of O_2 as reactive gas from room temperature to 900 °C at a heating rate of 10 °C min^{-1}. The thermogravimetric and differential thermogravimetric (TG-DTG) data were used to differentiate the oxidation behavior.

6.3.3 Catalyst activity tests

Activity measurement for steam reforming of tar was carried out in a fixed-bed quartz tube microreactor (i.d. ∅ 6 mm). Toluene was selected as a tar model compound because it contains both aromatic moiety (phenyl) and aliphatic moiety (methyl). Typically, ca. 50 mg of catalyst sample diluted in 50 mg of α-$Al_2O_3$was packed between layers of quartz wool. The reactor was placed in an electric furnace equipped with K-type thermocouples. The catalyst bed temperature was monitored and controlled by Shinko temperature controllers. Before the activity test, the catalyst was reduced at 500 °C for 2 h under 50% H_2 in helium. Toluene was vaporized from a saturator at 5 °C using He as carrier gas. The concentration of toluene was maintained at 2000 ppmv and steam to carbon ratio of 5. The total flow rate of feed gases was kept at 100 ml min^{-1} (GHSV = 20,000 h^{-1}) using Brook mass flow controllers. N_2 was used as an internal standard for chromatographic analyses. Measurements were carried out at furnace temperatures at 600-700 °C. The product gases were chromatographically analyzed using a Shimadzu GC 8A equipped with a CTR I (Altech) column and a TCD detector and a Shimadzu GC 17A equipped with a GSQ (Agilent technologies) column and an FID detector. The toluene conversion ($X_{C_7H_8}$), selectivities of carbon containing products (S_i) and hydrogen yield (Y_{H_2}) in this work were calculated as follow:

$$X_{C_7H_8}(\%) = \frac{[C_7H_8]_{in} - [C_7H_8]_{out}}{[C_7H_8]_{in}} \times 100 \quad (6.1)$$

$$S_{CO}(\%) = \frac{[CO]_{out}}{7\{[C_7H_8]_{in} - [C_7H_8]_{out}\}} \times 100 \quad (6.2)$$

$$S_{CO_2}(\%) = \frac{[CO_2]_{out}}{7\{[C_7H_8]_{in} - [C_7H_8]_{out}\}} \times 100 \quad (6.3)$$

$$S_{CH_4}(\%) = \frac{[CH_4]_{out}}{7\{[C_7H_8]_{in} - [C_7H_8]_{out}\}} \times 100 \quad (6.4)$$

$$S_{C_6H_6}(\%) = \frac{[C_6H_6]_{out}}{[C_7H_8]_{in} - [C_7H_8]_{out}} \times 100 \quad (6.5)$$

$$Y_{H_2}(\%) = \frac{[H_2]_{out}}{18[C_7H_8]_{in}} \times 100 \qquad (6.6)$$

where $[C_7H_8]_{in}$ and $[C_7H_8]_{out}$ is the concentration of toluene entering and leaving the reactor, respectively and $[CO]_{out}$, $[CO_2]_{out}$, $[CH_4]_{out}$, $[C_6H_6]_{out}$ and $[H_2]_{out}$ are the concentrations of carbon monoxide, carbon dioxide, methane, benzene and hydrogen leaving the reactor, respectively. N_2 was particularly used as an internal standard for chromatographic analyses.

6.4 Results and discussion

6.4.1 Catalyst characterizations

6.4.1.1 BET Surface Area and Metal Dispersion

The textural properties of Ni supported on mixed oxide catalysts are summarized in Table 6.1. It can be seen that the BET surface areas of Ni supported on mixed oxide samples are in the range of 57–72 $m^2\ g^{-1}$ and the average pore diameters of these samples are about 4.6–9.4 nm. It was noticed that the BET surface areas were decreased after incorporation of chromium, iron, manganese and vanadium. Particularly, the surface area of vanadium-containing sample was significantly decreased. This might be because the formation of $CeVO_4$ phase indicated by XRD.

The degree of dispersion of Ni supported on $Ce_{0.75}Zr_{0.25}O_2$ and $Ce_{0.75}Zr_{0.15}Me_{0.10}O_2$ mixed oxide catalysts are higher than that of Ni/α-Al_2O_3 catalyst (Table 6.2) indicating that Ni particles are better dispersed on $Ce_{0.75}Zr_{0.15}Me_{0.10}O_2$ mixed oxide supports than α-Al_2O_3 support. It was noticed that the dispersion degree decrease significantly when chromium, iron or vanadium is added into Ce/Zr mixed oxide samples. This might be because some part of Cr, Fe or V species is left on the surface of the mixed oxides and be decorating the surface of nickel particles.

Table 6.1 Textural properties of Ni-supported catalysts

Catalyst	BET surface area ($m^2 g^{-1}$)	Total pore volume ($cm^3 g^{-1}$)	Average pore diameter (nm)
15 % Ni/α-Al_2O_3	5.5	0.03	18.2
15 % Ni/$Ce_{0.75}Zr_{0.25}O_2$	72	0.11	7.0
15 % Ni/$Ce_{0.75}Zr_{0.15}Cr_{0.10}O_2$	67	0.09	4.6
15 % Ni/$Ce_{0.75}Zr_{0.15}Fe_{0.10}O_2$	68	0.11	5.6
15 % Ni/$Ce_{0.75}Zr_{0.15}Mn_{0.10}O_2$	67	0.12	6.3
15 % Ni/$Ce_{0.75}Zr_{0.15}V_{0.10}O_2$	57	0.17	9.4

Table 6.2 Degree of Ni metal dispersions and Ni crystallite size of the Ni-supported catalysts

Catalyst	Ni metal dispersion (%)	Ni crystallite size (nm)
15% Ni/α-Al_2O_3	0.47	39
15% Ni/$Ce_{0.75}Zr_{0.25}O_2$	2.88	22
15% Ni/$Ce_{0.75}Zr_{0.15}Cr_{0.10}O_2$	1.02	28
15% Ni/$Ce_{0.75}Zr_{0.15}Fe_{0.10}O_2$	1.06	27
15% Ni/$Ce_{0.75}Zr_{0.15}Mn_{0.10}O_2$	1.46	26
15% Ni/$Ce_{0.75}Zr_{0.15}V_{0.10}O_2$	0.71	30

6.4.1.2 XRD analysis

The XRD patterns of Ni over different supports after calcined at 500 °C are shown in Figure 6.1. Similar to the XRD patterns of $Ni/Ce_{0.75}Zr_{0.25}O_2$ catalyst, those of $Ni/Ce_{0.75}Zr_{0.15}Me_{0.10}O_2$ (Me = Cr, Fe, Mn or V) catalysts exhibited major peaks at about 29°, 33°, 48° and 56° (2θ) indicated a cubic fluorite structure of CeO_2 (Pengpanich *et al.*, 2002). No peak of chromium, iron, manganese or zirconium oxides is observed. This might be because the ionic radii of Cr^{3+} (6.2 nm.), Fe^{3+} (6.5 nm), Mn^{3+} (6.2 nm) and Zr^{4+} (8.4 nm) are smaller than that of Ce^{4+} (9.7 nm), therefore, dissolution in the ceria lattice would be possible at low doping concentrations for Cr, Fe, Mn and Zr. In addition, the several small peaks characteristic of NiO are observed at about 37° and 43° (2θ). With $Ni/Ce_{0.75}Zr_{0.15}V_{0.10}O_2$, line of $CeVO_4$ is also observed. The mean nickel crystallite sizes obtained from XRD data for Ni supported on mixed oxide samples were calculated by using Scherrer's equation. It was found that the average nickel crystallite sizes of nickel supported mixed oxide catalysts are in the range of 22–30 nm, which are smaller than those $Ni/\alpha\text{-}Al_2O_3$ (Table 6.2).

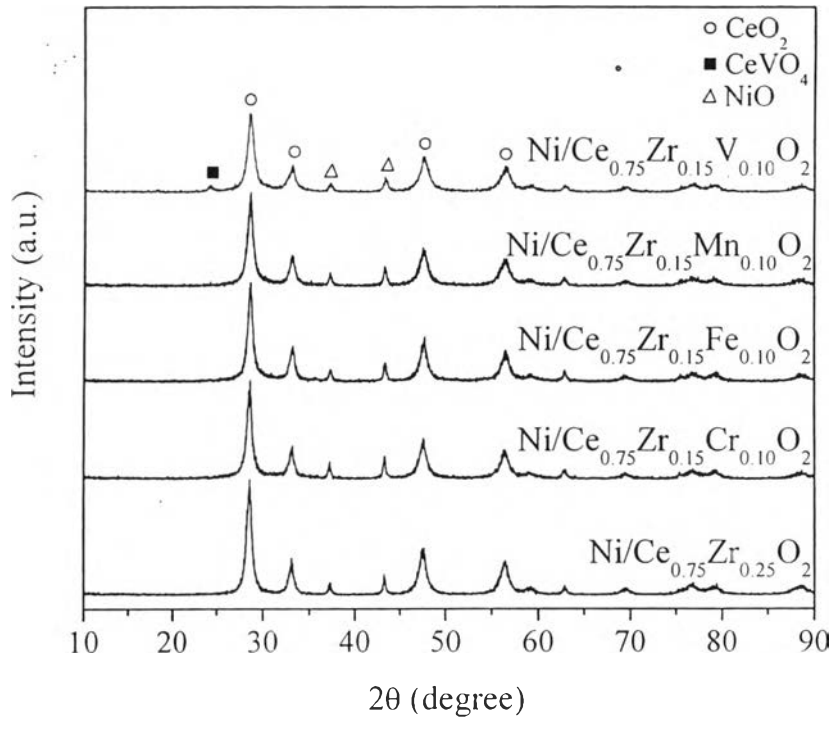

Figure 6.1 X-ray diffraction patterns for $Ni/Ce_{0.75}Zr_{0.25}O_2$ and $Ni/Ce_{0.75}Zr_{0.15}Me_{0.10}O_2$ (Me = Cr, Fe, Mn and V) mixed oxide catalysts with the aging time of 50 h, and calcined at 500 °C.

6.4.1.3 H_2-TPR

Figure 6.2 shows the H_2-TPR profiles of 15 wt% $Ni/Ce_{0.75}Zr_{0.25}O_2$, $Ni/Ce_{0.75}Zr_{0.15}Me_{0.10}O_2$ (Me = Cr, Fe, Mn and V) and Ni/α-Al_2O_3 catalysts. For $Ni/Ce_{0.75}Zr_{0.25}O_2$ catalyst, a broad peak at about 250-370 °C and another sharp peak at 460 °C were observed. The first peak is associated with the reduction of free NiO particles and the latter is related to the reduction of complex NiO species in intimate contact with the oxide support (Pengpanich *et al.*, 2004; Roh *et al.*, 2002). For the Ni/α-Al_2O_3 catalyst, only a broad peak attributed to agglomerated Ni is observed at 510 °C. The TPR profile of $Ni/Ce_{0.75}Zr_{0.15}Cr_{0.10}O_2$ catalyst showed two reduction peaks. The first reduction peak at 300 °C corresponds to the reduction of CrO_2 to Cr_2O_3 (Chen *et al.*, 1998; Khan *et al.*, 2008) and the second reduction peak at 520 °C corresponds to the reduction of NiO to Ni^0. It should be noted that the second peak reduction temperature of $Ni/Ce_{0.75}Zr_{0.15}Cr_{0.10}O_2$ catalysts is shifted to higher than those of $Ni/Ce_{0.75}Zr_{0.25}O_2$ catalysts indicating its less reducibility. This might be due to the fact that nickel particles having higher interaction with the $Ce_{0.75}Zr_{0.15}Cr_{0.10}O_2$ support. For $Ni/Ce_{0.75}Zr_{0.15}Fe_{0.10}O_2$ and $Ni/Ce_{0.75}Zr_{0.15}Mn_{0.10}O_2$ catalysts, the TPR features are in the similar manner of $Ni/Ce_{0.75}Zr_{0.25}O_2$. In the case of, however, the additional peak is observed at about 600 °C which is assigned to the reduction of Fe_3O_4 to FeO. For $Ni/Ce_{0.75}Zr_{0.15}V_{0.10}O_2$, three broad peaks at 330, 440 and 720 °C were observed which are the reduction of free NiO particles, the reduction of NiO to Ni^0 and the removal of oxygen from the bulk of $CeVO_4$, respectively (Yasyerli *et al.*, 2006).

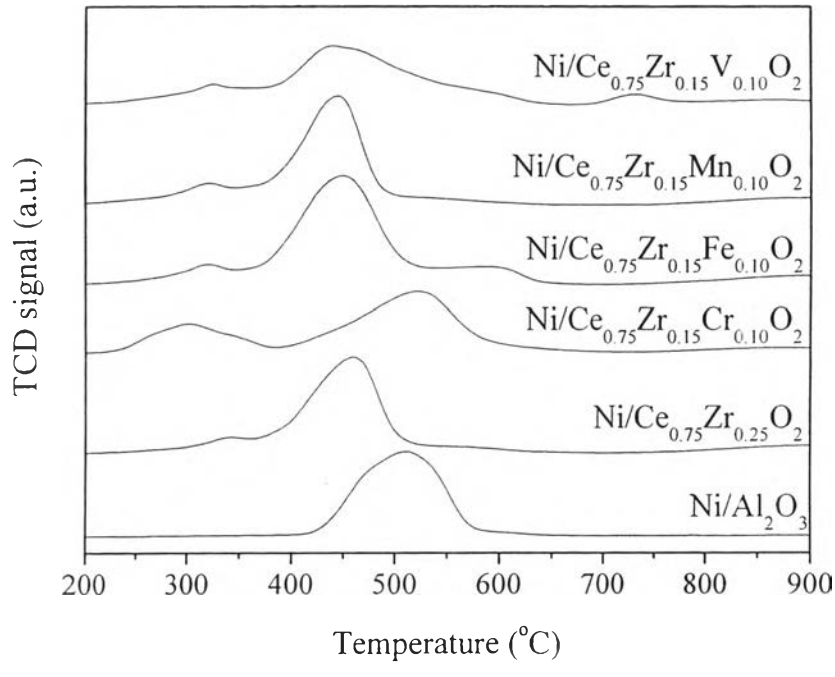

Figure 6.2 H_2-TPR profiles of the $Ni/Ce_{0.75}Zr_{0.25}O_2$, $Ni/Ce_{0.75}Zr_{0.15}Me_{0.10}O_2$ (Me = Cr, Fe, Mn and V) mixed oxide and 15% Ni/α-Al_2O_3 catalysts.

6.4.1.4 TEM

Figures 6.3-6.7 show the typical TEM images of nickel supported on $Ce_{0.75}Zr_{0.25}O_2$, and $Ce_{0.75}Zr_{0.15}Me_{0.10}O_2$ (Me = Cr, Fe, Mn and V) mixed oxide catalyst. From the TEM image of $Ni/Ce_{0.75}Zr_{0.25}O_2$, the particle size of the sample is almost in the range of 20-25 nm.

For nickel supported on $Ce_{0.75}Zr_{0.15}Me_{0.10}O_2$ (Me = Cr, Fe, Mn and V) catalysts, like $Ni/Ce_{0.75}Zr_{0.25}O_2$, the Ni particle sizes of the samples are not much changed when Cr, Fe, Mn and V incorporated into CeO_2-ZrO_2 mixed oxides. This result suggested that the addition of Cr, Fe, Mn and V does not change significantly the particle size of nickel. This result is in agreement with the average Ni crystallite size determined from XRD results.

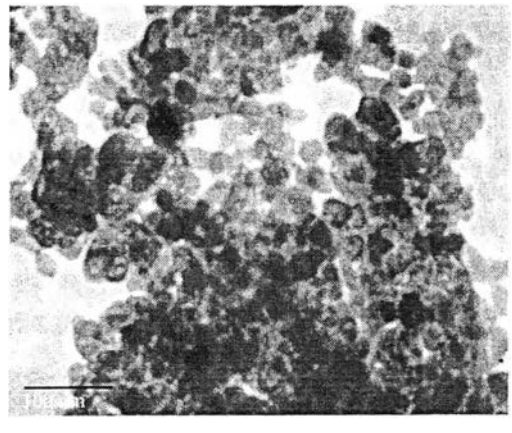

Figure 6.3 TEM image of $Ni/Ce_{0.75}Zr_{0.25}O_2$ catalyst.

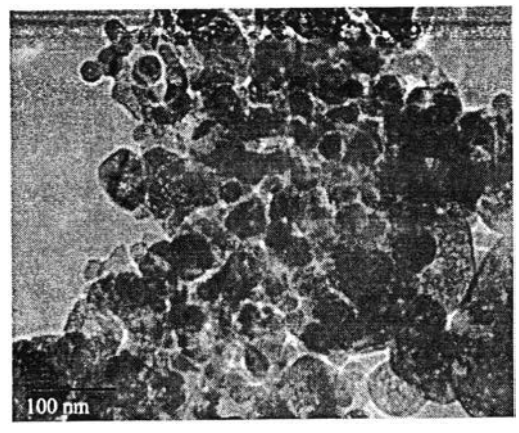

Figure 6.4 TEM image of $Ni/Ce_{0.75}Zr_{0.15}Cr_{0.10}O_2$ catalyst.

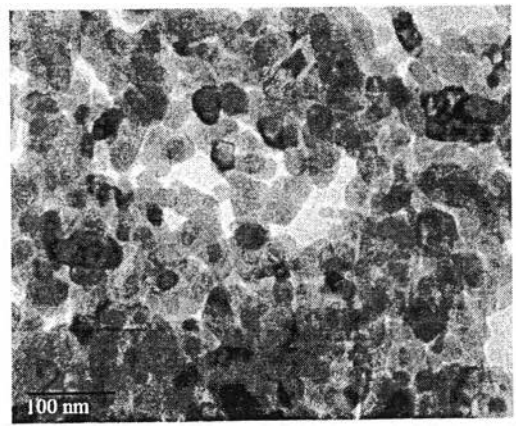

Figure 6.5 TEM image of $Ni/Ce_{0.75}Zr_{0.15}Fe_{0.10}O_2$ catalyst.

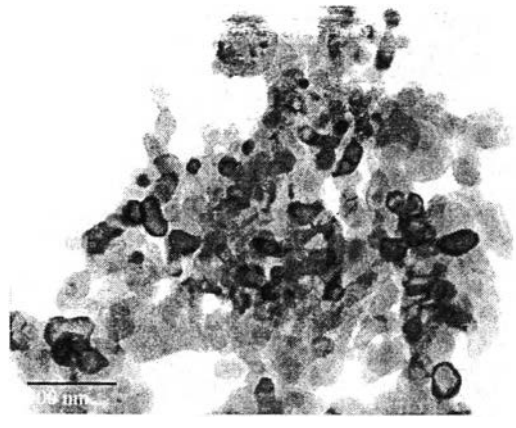

Figure 6.6 TEM image of $Ni/Ce_{0.75}Zr_{0.15}Mn_{0.10}O_2$ catalyst.

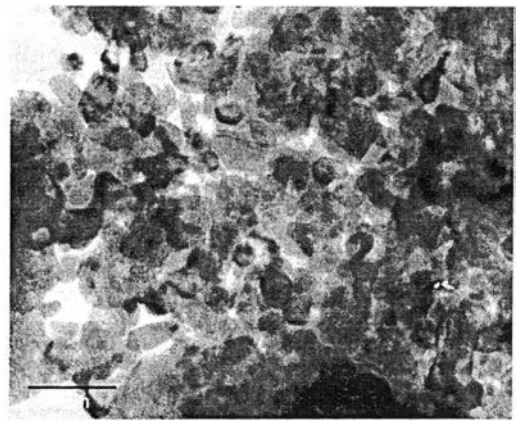

Figure 6.7 TEM image of $Ni/Ce_{0.75}Zr_{0.15}V_{0.10}O_2$ catalyst.

6.4.2 Catalytic Activities for Toluene Steam Reforming

Due to the reactor was clogged by deposited carbon as indicated by a dramatic increase in pressure drop across the reactor if the S/C equal to 2 and 3 were used. Thus, the catalytic activity tests for toluene steam reforming over nickel supported on mixed oxide catalysts were necessary to be carried out at the S/C equal to 5. Table 6.3 summarizes the activity and the gas production compositions upon steam reforming of toluene for $Ni/Ce_{0.75}Zr_{0.25}O_2$, $Ni/Ce_{0.75}Zr_{0.15}Me_{0.10}O_2$ (Me = Cr, Fe, Mn and V) mixed oxide and Ni/α-Al_2O_3 catalysts at 600 and 700 °C, respectively. Generally, the gas products are 19-31 vol.% CO, 1-11 vol.% CO_2, 68-71 vol.% H_2 and trace amount of CH_4 and C_6H_6. Based on the results, CO_2 and H_2 were also increased when Fe or Mn was incorporated into the CeO_2-ZrO_2 mixed oxide. This might be because the incorporation of Fe and Mn appears to promote the water-gas shift (WGS) reaction. At 600 °C, all $Ni/Ce_{0.75}Zr_{0.15}Me_{0.10}O_2$ catalysts achieve complete conversion of toluene, while $Ni/Ce_{0.75}Zr_{0.25}O_2$ and Ni/α-Al_2O_3 catalysts show 95% and 14% toluene conversion, respectively. This might be because the main carbon formation reaction ($2CO \leftrightarrow CO_2 + C$) is favorable at temperatures lower than 650 °C, indicating the deactivation by carbon deposition was occurred on $Ni/Ce_{0.75}Zr_{0.25}O_2$ and Ni/α-Al_2O_3 catalysts. On the other hand, 100% conversion of toluene was observed for the $Ni/Ce_{0.75}Zr_{0.25}O_2$ and $Ni/Ce_{0.75}Zr_{0.15}Me_{0.10}O_2$ catalysts at 700 °C. However, the differences in product gas compositions were still observed. It can be seen that $Ni/Ce_{0.75}Zr_{0.15}Me_{0.10}O_2$ catalysts, particularly $Ni/Ce_{0.75}Zr_{0.15}Mn_{0.10}O_2$, produce CO_2 higher than that of Ni/α-Al_2O_3 and $Ni/Ce_{0.75}Zr_{0.25}O_2$ catalysts. This is conformed to the existence of the WGS reaction.

6.4.3 Effect of Space-Time

The space-time was varied by changing the amount of catalyst for selected catalysts ($Ni/Ce_{0.75}Zr_{0.25}O_2$ and $Ni/Ce_{0.75}Zr_{0.15}Mn_{0.10}O_2$), at a given feed rate, with constant feed composition and temperature. Figure 6.8 and 6.9 show the influence of space-time on selectivity of carbon-containing products for toluene steam reforming over $Ni/Ce_{0.75}Zr_{0.25}O_2$ and $Ni/Ce_{0.75}Zr_{0.15}Mn_{0.10}O_2$ catalysts at 700

°C, respectively. It was found that the selectivities obtained at low space-times permitted identification of primary reaction products, i.e. CO, CH_4 and C_6H_6 resulting from steam reforming and dealkylation reactions. For both catalysts, an increase in space-time led to an increase in CO_2 selectivity, formed from CO via the WGS reaction (Świerczyński *et al.* 2007).

Table 6.3 Reaction characteristics of gas compositions using various nickel supported on $Ce_{0.75}Zr_{0.25}O_2$, $Ni/Ce_{0.75}Zr_{0.15}Me_{0.10}O_2$ mixed oxide and α-Al_2O_3 catalysts at reaction temperature of 600 and 700 °C (time on stream = 6 h; S/C ratio = 5.0)

Catalyst	Reaction temperature (°C)	Conversion (%)	Gas composition (%)				
			CO	CO_2	CH_4	C_6H_6	H_2
15% Ni/α-Al_2O_3	600	14	28.9	2.9	1.0	0.03	67.2
15% $Ni/Ce_{0.75}Zr_{0.25}O_2$		95	27.0	3.9	1.2	0.02	67.9
15% $Ni/Ce_{0.75}Zr_{0.15}Cr_{0.10}O_2$		100	25.2	5.1	0.6	0.01	69.1
15% $Ni/Ce_{0.75}Zr_{0.15}Fe_{0.10}O_2$		100	23.7	6.7	0.0	0.0	69.6
15% $Ni/Ce_{0.75}Zr_{0.15}Mn_{0.10}O_2$		100	18.6	11.3	0.0	0.0	70.1
15% $Ni/Ce_{0.75}Zr_{0.15}V_{0.10}O_2$		100	24.3	5.4	0.5	0.01	69.8
15% Ni/α-Al_2O_3	700	77	30.5	0.8	0.0	0.01	69.7
15% $Ni/Ce_{0.75}Zr_{0.25}O_2$		100	27.5	2.6	0.0	0.0	69.9
15% $Ni/Ce_{0.75}Zr_{0.15}Cr_{0.10}O_2$		100	25.7	4.2	0.0	0.0	70.1
15% $Ni/Ce_{0.75}Zr_{0.15}Fe_{0.10}O_2$		100	23.8	6.0	0.0	0.0	70.2
15% $Ni/Ce_{0.75}Zr_{0.15}Mn_{0.10}O_2$		100	20.7	8.2	0.0	0.0	71.1
15% $Ni/Ce_{0.75}Zr_{0.15}V_{0.10}O_2$		100	25.2	4.3	0.0	0.0	70.5

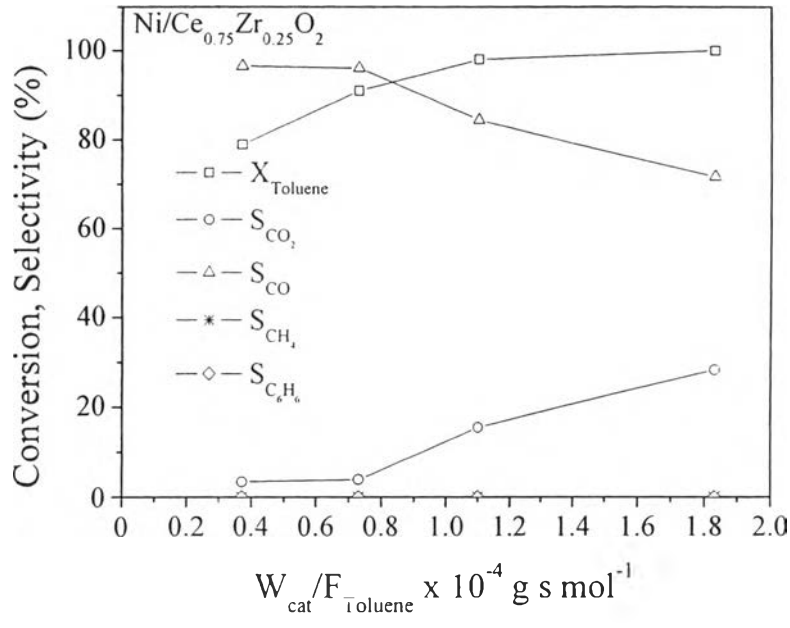

Figure 6.8 Influence of space-time on toluene conversion and selectivity to carbon-containing products during steam reforming of toluene over $Ni/Ce_{0.75}Zr_{0.25}O_2$ catalyst; with a gas mixture composed of 2000 ppmv C_7H_8, S/C ratio = 5.0, T = 700 °C and time on stream = 6 h.

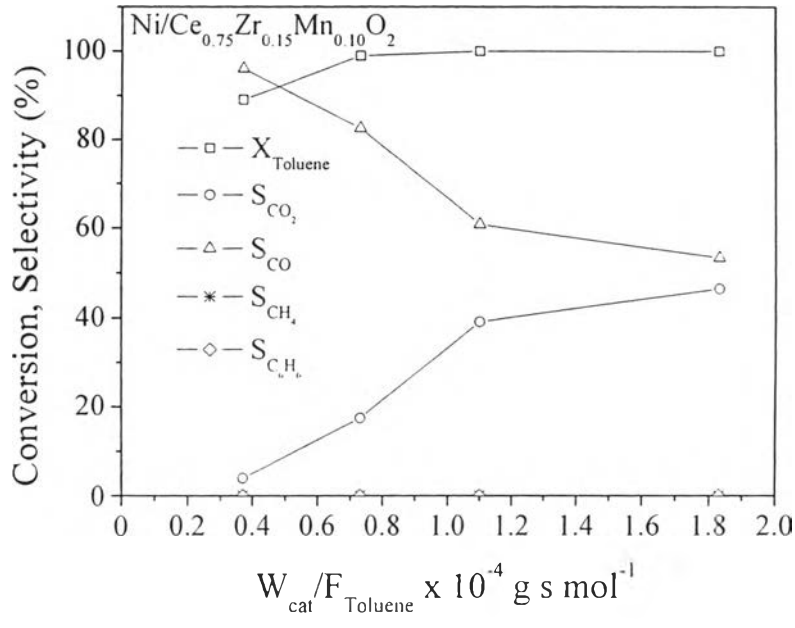

Figure 6.9 Influence of space-time on toluene conversion and selectivity to carbon-containing products during steam reforming of toluene over $Ni/Ce_{0.75}Zr_{0.15}Mn_{0.10}O_2$ catalyst; with a gas mixture composed of 2000 ppmv C_7H_8, S/C ratio = 5.0, T = 700 °C and time on stream = 6 h.

6.4.4 Carbon Formation

The catalytic activities and stabilities of $Ni/Ce_{0.75}Zr_{0.25}O_2$, $Ni/Ce_{0.75}Zr_{0.15}Me_{0.10}O_2$ (Me = Cr, Fe, Mn and V) catalysts for steam reforming of toluene were compared with those of Ni/α-Al_2O_3 catalyst at reaction temperature of 600 and 700 °C as shown in Figures 6.10 and 6.11, respectively. At 600 °C, it was found that the complete toluene conversions of $Ni/Ce_{0.75}Zr_{0.15}Me_{0.10}O_2$ (Me = Cr, Fe, Mn and V) catalysts remained unchanged for at least 6 h on stream whereas a rapid deactivation was observed for Ni/α-Al_2O_3 catalyst after 0.5 h on stream. For $Ni/Ce_{0.75}Zr_{0.25}O_2$ catalyst, the initial activity for steam reforming of toluene was almost 100%, however, the toluene conversion slightly decreased after 2 h on stream. This suggests that the $Ni/Ce_{0.75}Zr_{0.15}Me_{0.10}O_2$ (Me = Cr, Fe, Mn and V) catalysts be rather high active and stable for the steam reforming of toluene. It is believed that the improvement of reducibility and good oxidation ability of the $Ce_{0.75}Zr_{0.15}Me_{0.10}O_2$ (Me = Cr, Fe, Mn and V) mixed oxide supports appears to play a role in promoting the oxidation of carbon precursors on the nickel surface.

The amounts of carbon deposited on the spent catalysts were determined as summarized in Table 6.4. It is indicated that the Mn-doped catalysts possess the lowest amounts of carbon formed (ca. 1.2%) as compared to those formed on the Ni/α-Al_2O_3, $Ni/Ce_{0.75}Zr_{0.25}O_2$, $Ce_{0.75}Zr_{0.15}Cr_{0.10}O_2$, $Ce_{0.75}Zr_{0.15}Fe_{0.10}O_2$ and $Ce_{0.75}Zr_{0.15}V_{0.10}O_2$ catalysts (41.7% and 16.2%, 7.3%, 1.8% and 5.2%, respectively). It is believed that the modification of Ni/CeO_2-ZrO_2 catalysts with Mn incorporation helps prevent the carbon deposition by promoting the surface carbon gasification and/or WGS reaction.

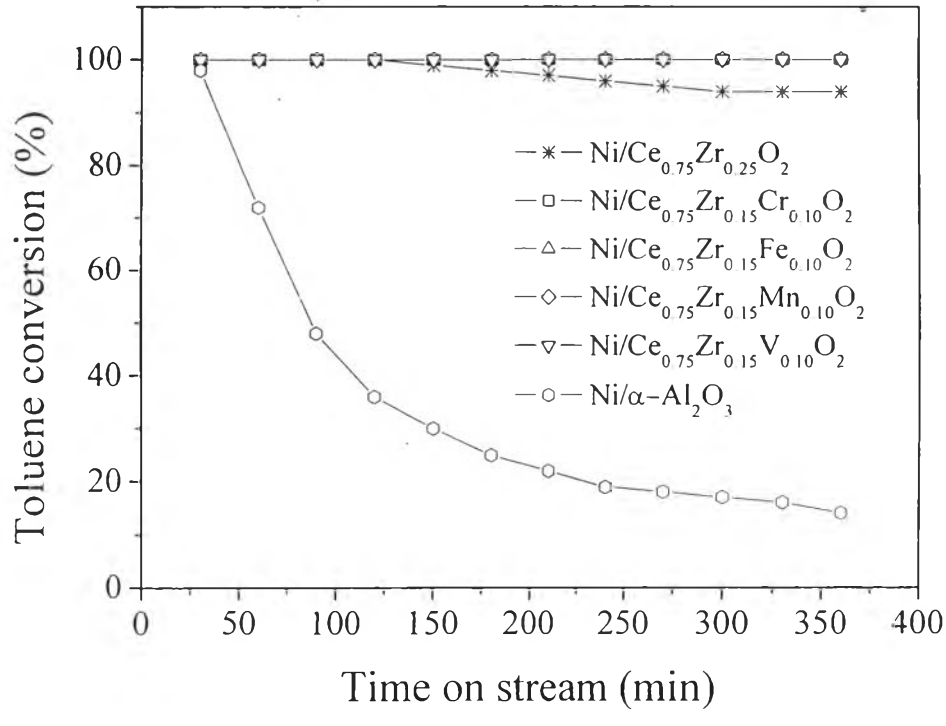

Figure 6.10 Catalytic activity for toluene steam reforming over $Ni/Ce_{0.75}Zr_{0.25}O_2$, $Ni/Ce_{0.75}Zr_{0.15}Me_{0.10}O_2$ (Me = Cr, Fe, Mn and V) mixed oxide and 15% $Ni/\alpha\text{-}Al_2O_3$ catalysts; with a gas mixture composed of 2000 ppmv C_7H_8, S/C ratio = 5.0 and T = 600 °C.

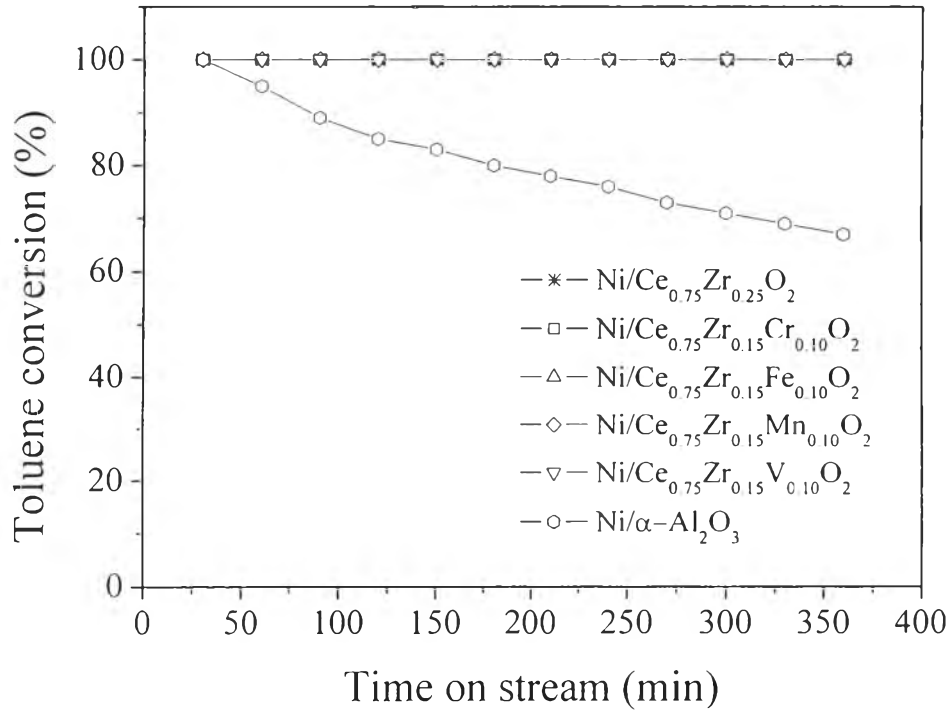

Figure 6.11 Catalytic activity for toluene steam reforming over $Ni/Ce_{0.75}Zr_{0.25}O_2$, $Ni/Ce_{0.75}Zr_{0.15}Me_{0.10}O_2$ (Me = Cr, Fe, Mn and V) mixed oxide and 15% $Ni/\alpha\text{-}Al_2O_3$ catalysts; with a gas mixture composed of 2000 ppmv C_7H_8, S/C ratio = 5.0 and T = 700 °C.

Table 6.4 Total amounts of carbon deposited on catalysts via the toluene steam reforming; after 6 h on stream, at 700 °C and, an S/C ratio of 5.0

Catalyst	Carbon formation (%)
15% $Ni/\alpha\text{-}Al_2O_3$	41.7
15% $Ni/Ce_{0.75}Zr_{0.25}O_2$	16.2
15% $Ni/Ce_{0.75}Zr_{0.15}Cr_{0.10}O_2$	7.3
15% $Ni/Ce_{0.75}Zr_{0.15}Fe_{0.10}O_2$	1.8
15% $Ni/Ce_{0.75}Zr_{0.15}Mn_{0.10}O_2$	1.2
15% $Ni/Ce_{0.75}Zr_{0.15}V_{0.10}O_2$	5.2

6.5 Conclusions

In conclusion, the $Ni/Ce_{0.75}Zr_{0.15}Me_{0.10}O_2$ (Me = Cr, Fe, Mn and V) mixed oxide catalysts exhibit high activities and stabilities for toluene steam reforming at least 6 h during the course of the experiments with no sign of deactivation, unlike $Ni/\alpha\text{-}Al_2O_3$, which showed the deactivation after 0.5 h on stream. Particularly, the incorporation of Mn into $Ni/CeO_2\text{-}ZrO_2$ catalyst decreases the amounts of carbon deposition and maintains the catalytic activity for steam reforming of toluene. It is believed that the addition of Mn appears to improve the catalytic activity and stability due to its high oxygen mobility and/or oxidation ability of $Mn^{2+,3+}$, allowing gasification and/or oxidation of deposited carbon.

6.6 Acknowledgements

This work was supported by the Thailand Research Fund (under Waste-to-Energy project and Royal Golden Jubilee Ph.D. Program: Grant 0170/46), and the Research Unit for Petrochemical and Environmental Catalysts, Ratchadapisek Somphot Endowment Fund, and the National Center of Excellence for Petroleum, Petrochemicals and Advanced Materials, Chulalongkorn University.

6.7 References

Abu El-Rub. Z., Bramer, E.A., Brem, G. Review of catalysts for tar elimination in biomass gasification processes. Industrial and Engineering Chemistry Research, 43, 6911-6919.

Baker, E.G., Mudge, L.K., Brown, M.D. (1987) Steam gasification of biomass with nickel secondary catalysts. Industrial and Engineering Chemistry Research, 26, 1335-1339.

Bampenrat, A., Meeyoo, V., Kitiyanan, B., Rangsunvigit, P., Risksomboon, T. (2009) Naphthalene steam reforming over Mn-doped CeO_2-ZrO_2 supported nickel catalysts. Applied Catalysis A: General, Submitted.

Chen, J., Wu, Q., Zhang, J., Zhang, J. (2008) Effect of preparation methods on structure and performance of $Ni/Ce_{0.75}Zr_{0.25}O_2$ catalysts for CH_4–CO_2 reforming. Fuel, 87, 2901-2907.

Chen, P., Zhang, H.-B., Lin, G.-D., Tsai, K.-R. (1998) Development of coking-resistant Ni-based catalyst for partial oxidation and CO_2-reforming of methane to syngas. Applied Catalysis A: General, 166, 343-350.

Dayton, D. (2002) Review of the literature on catalytic biomass tar destruction: Milestone completion report. NREL/TP-510-32815, National Renewal Energy Laboratory.

Duarte de Farias, A.M., Bargiela, P., Rocha, M.G., Fraga, M. (2008) Vanadium-promoted Pt/CeO_2 catalyst for water-gas shift reaction. Journal of Catalysis, 260, 93-102.

Etsell, T.H., Flengas, S.N. (1970) Electrical properties of solid oxide electrolytes. Chemical Reviews, 70, 339-376.

Garcia, L., French, R., Czernik, S., Chornet, E. (2000) Catalytic steam reforming of bio-oils for the production of hydrogen: effect of catalyst composition. Applied Catalysis A: General, 201, 225-239.

Khan, A., Smirniotis, P.G. (2008) Relationship between temperature-programmed reduction profile and activity of modified ferrite-based catalysts for WGS reaction. Journal of Molecular Catalysis A: Chemical, 280, 43-51.

Li, C., Hirabayashi, D., Suzuki, K. (2009) Development of new nickel based catalyst for biomass tar steam reforming producing H_2-rich syngas. Fuel Processing Technology, 90, 790-796.

Miyazawa, T., Kimura, T., Nishikawa, J., Kado, S., Kunimori, K., Tomishige, K. (2006) Catalytic peerformance of supported Ni catalysts in partial oxidation and steam reforming of tar derived from the pyrolysis of wood biomass. Catalysis Today, 115, 254-262.

Park, H.J., Park, S.H., Sohn, J.M., Park, J., Jeon, J.-K., Kim, S.-S., Park, Y.-K. (2009) Steam reforming of biomass gasification tar using benzene as a model compound over various Ni supported metal oxide catalysts. Bioresource Technology, In press.

Pengpanich, S., Meeyoo, V., Risksomboon, T., Bunyakiat, K. (2002) Catalytic oxidation of methane over CeO_2-ZrO_2 mixed oxide solid solution catalysts prepared via urea hydrolysis. Applied Catalysis A: General, 234, 221-233.

Pengpanich, S., Meeyoo, V., Risksomboon, T. (2004) Methane partial oxidation over Ni/CeO_2–ZrO_2 mixed oxide solid solution catalysts. Catalysis Today, 93-95, 95-105.

Roh, H.-S., Jun, K.-W., Dong, W.-S., Chang, J.-S., Park, S.-E., Joe, Y.-I. (2002) Highly active and stable Ni/Ce–ZrO2 catalyst for H_2 production from methane. Journal of Molecular Catalysis A: Chemical, 181, 137-142.

Sato, K., Fujimoto, K. (2007) Development of new nickel based catalyst for tar reforming with superior resistance to sulfur poisoning and coking in biomass gasification. Catalysis Communications, 8, 1697-1701.

Srinakruang, J., Sato, K., Vitidsant, T., Fujimoto, K. (2006) Highly efficient sulfur and coking resistance catalysts for tar gasification with steam. Fuel, 85, 2419-2426.

Sutton, D., Kelleher, B., Ross, J.R.H. (2001) Review of literature on catalysts for biomass gasification. Fuel Processing Technology, 73, 155-173.

Świerczyński, D., Libs, S., Courson, C., Kiennemann, A. (2007) Steam reforming of tar from a biomass gasification process over Ni/olivine catalyst using toluene as a model compound. Applied Catalysis B: Environmental, 74, 211-222.

Yasyerli, S., Dogu, G., Dogu, T. (2006) Selective oxidation of H_2S to elemental sulfur over Ce-V mixed oxide and CeO_2 catalysts prepared by the complexation technique. Catalysis Today, 117, 271-278.